ELASTOTHERMAL ANALYSIS OF THE CAST IRON PLATE IN AN ECOLOGICAL WOOD STOVE

Danilo de Souza Braga
Daniel Freitas Coelho
Universidade Federal do Pará, Grupo de Vibrações e Acústica. Rua Augusto Corrêa, 01 - Guamá. Belém - Pará – Brasil
danilo.braga@itec.ufpa.br
daniel.coelho@itec.ufpa.br

Newton Sure Soeiro
Universidade Federal do Pará, Grupo de Vibrações e Acústica. Rua Augusto Corrêa, 01 - Guamá. Belém - Pará – Brasil
nsoeiro@ufpa.br

Gustavo da Silva Vieira de Melo
Universidade Federal do Pará, Grupo de Vibrações e Acústica. Rua Augusto Corrêa, 01 - Guamá. Belém - Pará – Brasil
gmelo@ufpa.br

Sergio Aruana Elarrat Canto
Universidade Federal do Pará, Energia Biomassa e Meio Ambiente. Rua Augusto Corrêa, 01 - Guamá. Belém - Pará – Brasil
aruana@ufpa.br

Matthieu Lalau
Ensam Paris Tech, 147 boulevard de l Hopital 75013. Paris - France
matthieu.lalau@gmail.com

Abstract. Current researches indicate that millions of people around the world use wood stoves, especially those living in rural areas and with low income. This happens because the stoves manufacturing process uses a low-tech both raw material acquisition and stove operation, and there is still availability of low-cost firewood to ensure these users some autonomy. However, these advantages lead to production of low-efficiency stoves that are harmful to human health and the environment, by emitting toxic substances and pollutants. Ecofogão is one of the companies that produce these stoves, which have the peculiarity of heating a pan with heat transmission through a cast iron plate, which increases energy efficiency and prevents contamination of indoor air by using a chimney to evacuate gases from the burning of biomass. This paper discusses the structural behavior of the iron plate against the heat flux received in regional conditions operation, employing computational structural simulations based in finite element method (FEM), with the goal of providing subsidies to the plate design to resist better the generated stresses, avoiding cracks, warping and even facilitate the specification of materials most suitable for working conditions.

Keywords: Stress analysis, elastothermal analysis, biomass, ecological stove.

1. INTRODUCTION

The present millions of people around the world use wood stoves make the research on biomass stove has grew broadly and was established in late 1980s. It is necessary to promote research and development in the field of cook stove to obtain better thermal efficiency and lower emissions to this people (Ravi *et al*, 2002).. Thus, clearly, the objective was to optimize stove geometry so that the performance of the stove could be improved. According to Gupta and Mittal (2010), the outcome of numerous such studies helped building a data base regarding various issues related to design, development, performance and construction of cook stoves. These design modifications essentially included improvement of flow passages to achieve enhanced momentum, permitting preheating of air for heat recovery. Gupta and Mittal (2010) simulate the buoyancy induced flow in an analogue of a single pan wood stove. In the present analysis, flow through fuel bed is modeled as flow through porous medium and heat release in the bulk fluid due to combustion is represented by uniform generation of heat.

Furthermore, analysis of stresses from the thermal loading is taken into account during the design phase. Mechanical failures can occur for both the elastic regime as plastic. Thus, sequentially coupled approach is used for thermo-mechanical problem and the problem is divided into two parts, heat analysis and thermal stress analysis.

Mostly, the first is based on the computational fluid dynamics (CFD) models which were known to be proven scientific tool and widely used to replace time consuming and expensive experimental work, which it is consisted of equations of continuity, momentum and energy and are solved numerically to heat analysis. Thus, the CFD simulation of wood stove would subsequently provide necessary input such as mass flow rates, heat transfer to pan, thermal efficiency to the model to be developed eventually.

The second, according to Aziz and Tao (2012) and Mackin *et al* (2002) that developed a simulation of thermal stresses in a disc brake, the finite element analysis (FEA) is performed to determine the temperatures profile in the disc and to analyze the stresses for the repeated braking, which could be used to calculate the fatigue life of a disc. To calibrate the model obtained, it is necessary compare numerical results with the experimental results. Bhadanri *et al* (1988) realize an experimental investigation of a single pot wood-burning stove. The stove incorporates features such as a converging combustion space, a grate, preheated secondary air and a swirling-device. These results, for example, can be modeled numerically to test the prediction of boundary condition on CFD model. Kohli (1992) and Kohli *et al* (1993) developed the sub-model for buoyancy induced flow in the configuration sawdust stove cross section and model cross section. An experimental rig for measuring the mass flow rate through the configuration was designed, fabricated and calibrated to validate the predictions of the submodel (Kohli *et al*, 2002).

In this sense, the present paper explore an investigation about numerical elastothermal analysis of the cast iron plate in an ecological wood stove from heat transfer loads on steady operational conditions. Initially, the flows of combustion gases are treated as nitrogen. The calibrated CFD model is created to quantify the thermal loads. And then, the structural behavior of the iron plate against the heat flux received, employing computational structural simulations based in finite element method (FEM). The studies performed on the laboratory helps understanding the rupture of the plate in use, similarly to the manufacturer reports. From the chemical and metallographic analysis, is observed concentration of elements is highly elevated, which means a exacerbated graphitization, a type of vermicular graphite quantitatively high, compromising the plate mechanical proprieties. From this, the plate design to resist better the generated stresses, avoiding cracks, warping and even facilitate the specification of materials most suitable for working conditions are discussed.
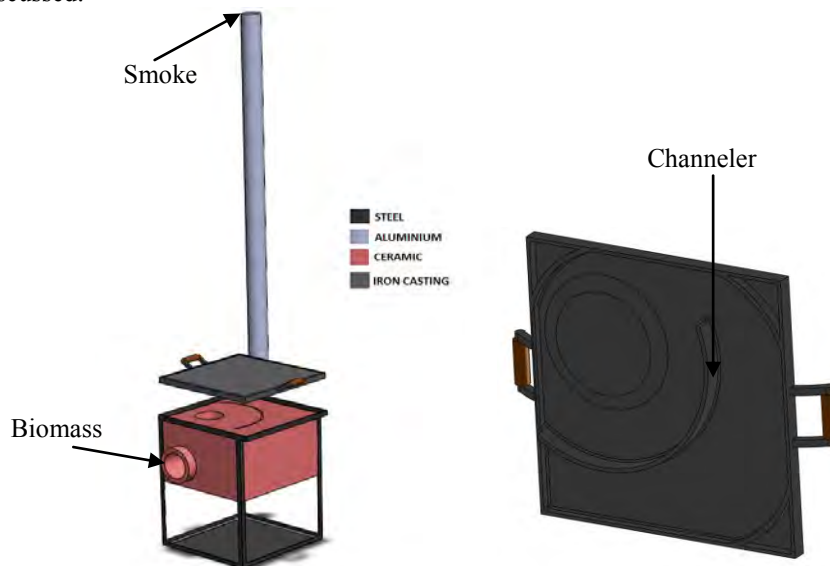
Figure 1. Wood stove and plate used as study case.

2. MATHEMATICAL MODEL AND COMPUTATIONAL DETAILS

The thermo mechanical problem is solved in uncoupled way; the temperature is calculated by solving thermal problem. Mechanical problem is solved to find the stresses and strains by using the temperature as known data. The temperature distribution in the material is first determined for calculating the thermal stresses within the material.

2.1 Contributing roles of conduction, convection, and radiation

According to Zube (2010) each heat transfer mode is split into two categories: losses and gains. The losses are associated with heat that is transferred into the stove body or out to ambient, while the gains are associated with heat that is transferred to the pot. A cross sectional view of the stove is provided for each heat transfer mode in Figure 2. Arrows drawn in each figure indicate the direction of heat transfer, noting that they are all pointing out of the control volume ($\dot{Q}_0$). The percentage values given represent the fraction of chemical energy contained in the fuel converted to heat that is either lost or gained.

Conductive heat transfer occurs through the floor of the stove to the ground, through the body of the stove to the surroundings, and through the thickness of the pot. There is zero energy gains associated with conduction heat transfer to the pot. The rate of steady state conduction heat transfer is defined by Eq. 1, where k = thermal conductivity, A = cross sectional area of object, ΔT = temperature difference, L = object thickness.

$$\dot{Q}_{cond} = \frac{k \cdot A \cdot \Delta t}{L} \tag{1}$$

Hot combustion gases interact with two separate surfaces: the inner surface of the stove (losses) and the outer surface of the pot (gains). The rate of steady state convection heat transfer is defined by Eq. 2, where h = convection coefficient (Wm^2/K), A = exposed surface area, ΔT = temperature difference.

$$\dot{Q}_{conv} = h \cdot A \cdot \Delta t \tag{2}$$

Convection coefficient (h) is a function of Nusselt number (Nu), gas thermal conductivity (k_{gas}), and diameter of the upper chamber stack (d) as defined by Eq. 3.

$$h = \frac{Nu \cdot k_{gas}}{d} \tag{3}$$

Nusselt number is a dimensionless temperature gradient at the surface, and is a function of Prandtl number (Pr) and Reynolds number as defined by Eq. 4 for a fully developed free jet impinging on a flat plate (Zube, 2010).

$$Nu = 0.565 \cdot Pr^{0.5} \cdot Re^{0.5} \tag{4}$$

Prandtl number (ratio of momentum and thermal diffusivities, $C_p\mu/k$) remains relatively constant while Reynolds number increases linearly with mass flow rate. The Reynolds number is a dimensionless variable that provides the ratio of inertial to viscous forces in a fluid, as provided by Eq. 5 where ρ = gas density, v = velocity, L = characteristic length (or diameter, D_h), μ = absolute viscosity.

$$Re = \frac{\rho \cdot v \cdot L}{\mu} \tag{5}$$

Typical flow properties through a cook stove tend to be either fully laminar or in the transition zone between laminar and turbulent. These regimes correspond to Reynolds numbers within the range of $500 < Re < 5000$ depending upon influences that include firepower, entrance effects, fuel obstruction, flame interaction and stove geometry.

Radiant energy originating from either the coal bed or flames is transferred to the stove body, pot, or ambient surroundings. The rate of blackbody radiation heat transfer between two surfaces is described by Eq. 6, where T_2 and T_1 are the respective temperatures of each surface.

$$\dot{Q}_{rad} = \varepsilon \cdot \sigma \cdot A \cdot (T_2^4 - T_1^4) \tag{6}$$

where ε is emissivity and σ is Blotzmann's constant ($5.70 * 10^{-8}$ W.m^{-2}.K^{-4}).
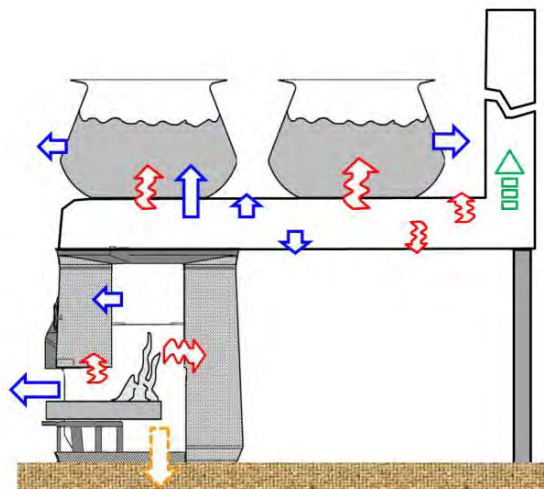
Figure 2. Steady state energy balance with heat transfer contributions. (Zube, 2010)

2.2 Heat transfer problem

According Gupta and Mittal (2010), the flow in the existing stove geometry is essentially non-axisymmetric in nature, so it can be modeled as 3D steady flow by allowing the stove geometry shown on Fig. 2. This was achieved by replacing the sideways primary air inlets by an axial entry through the stove bottom. Further, the secondary ports and fuel feed port are also replaced by a peripheral slot around the stove body having the same area as that of all the secondary air ports along with area of the fuel feed port put together. It is expected that this minor alteration of stove geometry would not alter the flow characteristics rustically and that the comparison of the predictions of our analysis with respect to the experimental behavior of original stove would still be valid.

The thermal problems are solved by using heat and fluid equation and first law of thermodynamics. Considering an isotropic solid body, the governing equation of problem is

$$\frac{\partial \rho}{\partial t} + \frac{\partial (\rho v_x)}{\partial x} + \frac{\partial (\rho v_y)}{\partial y} + \frac{\partial (\rho v_z)}{\partial z} = 0 \tag{7}$$

where ρ is the fluid density and v is the fluid velocity.

To incompressible fluid, ρ is constant, and then, the gradient of velocity is zero ($\nabla \cdot v = 0$). The equation of motion which prescribes the conservation of momentum is

$$\frac{\partial \rho v}{\partial t} + (\rho v)\nabla v = \nabla(-P\delta) + \nabla\left(\mu(\nabla v + (\nabla v)^T)\right) + S_M \tag{8}$$

where P is the static pressure, μ is the dynamic viscosity and S_M is the momentum source. So, the Navier-Stokes equations for cartesian coordinates are:

$$\rho \frac{\partial u}{\partial t} + \rho\left(v_x \frac{\partial u}{\partial x} + v_y \frac{\partial u}{\partial y} + v_z \frac{\partial u}{\partial z}\right) = F_x + \mu\left(\frac{\partial^2 v_x}{\partial x^2} + \frac{\partial^2 v_y}{\partial y^2} + \frac{\partial^2 v_z}{\partial z^2}\right) - \frac{\partial P}{\partial x}$$

$$\rho \frac{\partial v}{\partial t} + \rho\left(v_x \frac{\partial v}{\partial x} + v_y \frac{\partial v}{\partial y} + v_z \frac{\partial v}{\partial z}\right) = F_y + \mu\left(\frac{\partial^2 v_y}{\partial x^2} + \frac{\partial^2 v_y}{\partial y^2} + \frac{\partial^2 v_y}{\partial z^2}\right) - \frac{\partial P}{\partial y} \tag{9}$$

$$\rho \frac{\partial w}{\partial t} + \rho\left(v_x \frac{\partial w}{\partial x} + v_y \frac{\partial w}{\partial y} + v_z \frac{\partial w}{\partial z}\right) = F_z + \mu\left(\frac{\partial^2 v_z}{\partial x^2} + \frac{\partial^2 v_z}{\partial y^2} + \frac{\partial^2 v_z}{\partial z^2}\right) - \frac{\partial P}{\partial z}$$

Being F_x, F_y, F_z gravitational forces and u, v and w the components of velocity of the fluid. Considering an isotropic solid body, the governing equation of heat transfer (law of conservation of energy) problem is

$$\rho C_p\left(\frac{\partial T}{\partial t} + v_x \frac{\partial u}{\partial x} + v_y \frac{\partial u}{\partial y} + v_z \frac{\partial u}{\partial z}\right) = K\left(\frac{\partial^2 T}{\partial x^2} + \frac{\partial^2 T}{\partial y^2} + \frac{\partial^2 T}{\partial z^2}\right) \tag{10}$$

Being T the temperature, C_p the specific heat of the fluid and K is the thermal conductivity.

2.3 Thermoelasticity

When an isotropic material is subjected to a change in temperature, it will expands/contracts equally in all directions according thermoelasticity. Furthermore, when the material is loaded beyond its yield strength, plastic deformation occurs. The change in dimensions due to the temperature changes is called thermal strain, ε^{th} which is a function of (T-T_0), where T_0 is the initial temperature and T is the applied temperature. With exception of some materials, generally the material expands when it is heated and upon cooling it shrinks. Thermal strain is linear function of temperature change, defined by Aziz and Tao (2012) as

$$\varepsilon^{th} = \alpha(T)(T - T_0) \text{ and} \tag{11}$$

$$\varepsilon^{th} = \alpha(T)(T - T_{ref}) - \alpha(T_0)(T_0 - T_{ref}), \tag{12}$$

where $\alpha(T)$ is the thermal expansion coefficient and it is a temperature dependent property. The Eq. 11 is true when the initial temperature is equal to the reference temperature T_{ref}. If we have different reference and room temperatures, Eq. 12 has to be used.

If the material is free to move, internal stresses due to thermal strains are not produced, unlike mechanical strains which are related to internal stresses by the material constitutive law. Thus, to include the thermal strain in the linear elastic equation, the Cauchy stress equation needs to be introduced:

$$\sigma_{ij} = E_{ij}(\varepsilon - \varepsilon^{pl} - \varepsilon^{th}) \text{ or} \tag{13}$$

$$\sigma_{ij} = \delta_{ij}\lambda\varepsilon + 2G\varepsilon_{ij} - (3\lambda + 2G) - \alpha(T - T_{ref})\delta_{ij}, \tag{14}$$

where E_{ij} is known as the elasticity tensor (isotropic material is of symmetric properties), ε and ε^{pl} are the residual strain and plastic strain, respectively; G is known as shear modulus; δ_{ij} is Kronecker delta and is equal to 1 when i=j, otherwise is 0; λ is the scalar called Lame module. Lame module is written in terms of Young's modulus (E) and Poisson's ratio (γ) as

$$\lambda = \frac{\gamma E}{(1 + \gamma)(1 - 2\gamma)} \tag{15}$$

3. EXPERIMENTAL-NUMERICAL CALIBRATION

3.1 Experimental setup

It was performed in laboratory the measurement of the temperature on several points of the plate according to the scheme shown on Fig. 3. The temperature measurement was made using a laser pyrometer and a thermocouple. To measure the gas velocity, it was added a pitot tube on the outlet of the chimney (Fig. 4). The hypotheses adopted for the work were assumed that the mass flow rate is conserved and the fluid is incompressible: for any section, the mass flow rate can be deduced.
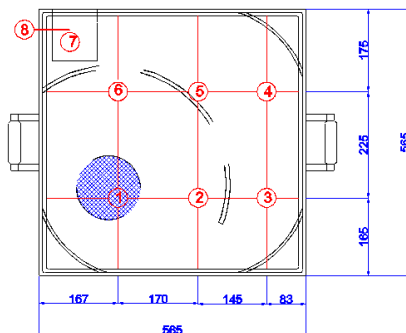
Figure 3. Measurement points of temperature
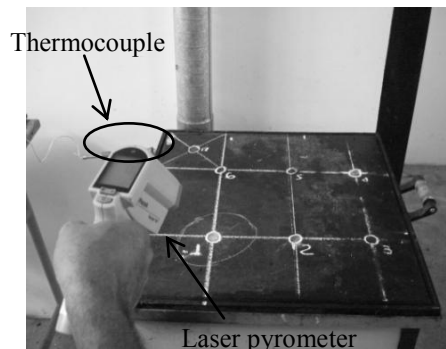
Figure 4. Measurement points with instruments

The biomass used is *jatobá* (abundant wood on the interior region of Pará), which are consumed initially 900 grams. Later, 120 grams are added in 20 minutes, 60 and 80 minutes after. The consumption of the biomass is 9.07 g/min during the first ten minutes and the mean consumption is 544 g/h. In total, 1.27 kg of *jatobá* was consumed. To characterize the fluid that will flow through the stove, gases analysis was performed, the results are shown on Table 1. The chemical formula of the biomass determined by the measurement was $C_{4,374}H_{5,476}O_{2,464}N_{0,124}S_{0,024}$. The results of that measurements show that nitrogen makes up the majority of the gas, about 70 % in mass, therefore it will be assumed to be the single component of the fluid on CFD simulation.

The experimental results obtained provide the temperatures of the points on the plate, identified as points 1, 2, 3, 4, 5, 6 e 7. The thermocouple results (point 8) show a large variation, because this point was located inside the stove where the turbulent behavior in this region decreases the equipment precision.

Table 1. Experimental results for gases analysis.

Specie	MW (kg/kmol)	m_i (kg)	N_i (kmol)	X_i	Y_i	Cp_i (kJ/kmol-K)	h_i (kJ/kmol)	s_i (kJ/kmol)	g_i (kJ/kmol)
CO_2	44.010	180.581	4.1032	0.16214	0.2434	60.94	-290700.85	314.689	-979333.69
CO	28.010	7.585	0.2708	0.01070	0.0107	36.539	-46948.55	261.897	-620056.55
H_2O	18.015	58.378	3.2405	0.12805	0.0787	52.311	-159298.63	269.345	-748706.73
H_2	2.016	0.083	0.0412	0.00163	0.0001	34.864	59477.44	191.445	-359462.31
H	1.008	0.005	0.0054	0.00021	0.0000	20.786	257270.63	156.039	-84189.63
OH	17.007	1.002	0.1743	0.00233	0.0014	35.149	99334.8	245.388	-437646.93
$O2$	31.999	5.576	0.0054	0.00689	0.0075	38.224	66325.67	272.079	-529065.58
O	15.999	0.084	0.0589	0.00021	0.0001	20.824	288833.52	203.013	-155418.65
N_2	28.010	485.350	0.1743	0.68471	0.6542	36.282	62937.91	255.239	-495600.36
NO	30.004	1.665	0.0555	0.00219	0.0022	36.897	155083.7	276.359	-449672.15
SO_2	64.059	1.537	0.0240	0.00095	0.0021	58.621	-194622.97	350.185	-960932.79
CH_4	16.043	0.000	0.0000	0.00000	0.0000	96.506	66654.94	314.344	-621223.74
AIR	39.948	0.000	0.0000	0.00000	0.0000	20.786	39289.17	196.166	-389980.56
He	4.003	0.000	0.0000	0.00000	0.0000	20.786	39289.17	167.475	-327197.22
Ash	---	0.000	---	---	0.0000	---	---	---	---
Products	29.314	741.846	25.31	1	1	42.36	-23885.98	245.388	-437646.93

$(T_p$=2188 K; P_{prod}=1atm)
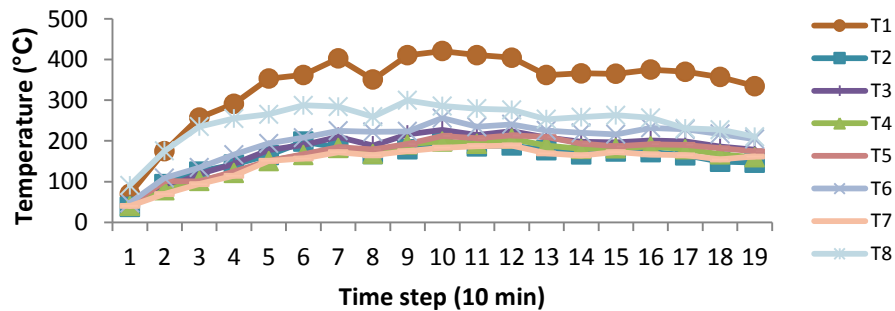
Figure 5. Measured temperature on specified points.

As can be observed on Figure 5, there is a time to reach steady characteristics of temperature. After 90 minutes, the temperatures remain nearly constant: this time step will be used for the numerical steady simulation. So, the mean velocity on the outlet of the chimney is 4 m/s, measured with pitot tube. The experimental data measured was used to compare with numerical data. The nitrogen proprieties (See Table 2) were introduced on CFD calculation in order to export the temperatures on the plate from fluid convection.

Table 2. Nitrogen proprieties.

Fluid proprieties	
μ [kg/(m.s)]	$1.6633e^{-5}$
k [W/(m.K)]	0.0204
Outlet velocity [m/s]	4
ρ [kg/m^3]	1.138
Cp [J/(kg.k)]	1040.63

3.2 Boundary conditions

It is permissible to specify the properties of the flow, on the inlet and outlet. For mathematical accuracy, would have to know the values of velocity, pressure and temperature for each point, in the planes on the inlet and outlet, however mostly this is impractical. Instead, the equations of motion are simplified, until it is less necessary the knowledge of boundary regions.

Flow in biomass stoves is entirely due to natural convection, with rare exceptions of stoves using a mechanical draught of air. Kohli [1992] points out that it has been an inherent shortcoming of most stove models in the literature that they tend to use correlations which are strictly valid only for fully developed forced flows to estimate the mass flow rate of air through the stove. By accounting for natural convection, it was shown that the predictions of heat transfer efficiency of a stove were in better agreement with the experimentally measured values. To simulate buoyancy-induced flow in a stove, one needs to solve the Navier-Stokes equations, which are the equations of conservation of momentum, simultaneously with the equations of conservation of mass and energy, with the appropriate boundary conditions.

3.2.1 At the inlet

At the inlet, the stagnation pressure is the ambient pressure at the same elevation. Then, neglecting the viscous losses due to acceleration of the fluid from surroundings to the stove inlet, Bernoulli equation can be used to express the static fluid pressure P in terms of velocity v (Gupta and Mittal, 2010). Further, the fluid is assumed to enter the stove axially, thus, radial velocity at the inlet is taken to be zero. Then, continuity equation dictates that the normal gradient of axial mass flux should also be zero. The temperature at the stove inlet can be assumed to be the temperature to burn the wood, then,

$$P_t = P + \frac{\rho}{2}\left(\frac{Q}{A_{inlet}}\right)^2, T_{inlet} = 1200\ °\text{C}, \theta = 0\ (axial) \tag{16}$$

In some situations, it is suitable to specify a uniform value of the amount of turbulence on inlet regions. The turbulence can be determined by the turbulence intensity, shown on Eq. 17. Where u' is the root mean square of the velocity fluctuations, v_{avg} is the average velocity of the flow on the inlet and Re_{D_h} is the Reynolds number for a duct with D_h diameter.

$$I = \frac{v'}{v_{avg}} = 0.16\left(Re_{D_h}\right)^{-1/8} \tag{17}$$

Another parameter to determinate is the turbulence length scale (l), which is a physical quantity describing the size of the large energy-containing eddies in a turbulent flow. An approximation between l and the physical size of the duct is defined by Eq. 13.

$$l = 0.07D_h \tag{18}$$

To the study case (D_h= 0.14 m), were obtained to turbulence intensity and length scale values of 0.043 and 9.8e-3 m, respectively, which was introduced on this model.

3.2.2 At the stove exit

The exhaust gases leaving the combustion chamber can be treated as a jet entering a still medium i.e. static pressure is equal to the local ambient pressure, however, if outlet velocity is considerable, it will have to be taken in account. Also, assuming that the flow leaves the exit axially, consequently, axial velocity is the same measured with the pitot tube. Thus, boundary conditions at the exit can be written as;

$$v_{outlet} = v_{measured} = 4\ m/s, \theta = 0\ (axial) \tag{19}$$

3.2.3 At the solid wall

Flow inside of the stove is surrounded by 2 elements: an iron cast plate and ceramic block (See Fig. 1). Both the boundaries are considered as solid walls. On these boundaries, were applied the no slip condition of the flow and convective boundary condition is also imposed. On the bottom, on ceramic part, heat changes are considered to be negligible or adiabatic. On top, it is used the heat transfer coefficient calculated for the region of the plate considering the outside temperature. Same form, the heat transfer coefficient was calculated to chimney region.

In the chimney, heat transfer is done by: conduction, convection and radiation. So it is necessary to calculate the convection heat transfer coefficient knowing Nusselt, Prandtl and Reynolds numbers for flow inside the tube. In other hand, to calculate the mean convection heat transfer coefficient for the plate, it is considered the flow between the two plates, having 15 mm thickness. These data is shown on Table 3 and 4 for the plate and chimney respectively. It is seen that the behavior of gas under the plate is more complex than the chimney, due to its geometry, which gives a curved path to nitrogen gas.

Table 3. Heat transfer mean coefficient on plate.

Number	Results
Reynolds number	8212
Prandtl number	0.855
Nusselt number	30
h [W/(m.K)]	20

Table 4. Heat transfer mean coefficient on chimney.

Number	Results
Reynolds number	26000
Prandtl number	0.855
Nusselt number	61.32
h [W/(m.K)]	13

To determine the temperature field on the surface of the plate, it was introduced radiation and conduction effects, not measured on CFD calculation. For the plate material it was inserted emissivity ($\mathcal{E}$) equals to 0.8 and convective heat transfer coefficient (h) equals to 5 Wm^{-2} ^{o}C^{-1}.

3.3 Turbulence model

The k-ε model can be used because it is the simplest with the fastest processing, however needs a reasonable pressure gradient. The turbulence model (k-ε) has provided good results to numerical models involving the turbulence and has presented good strength in solutions of the equations of motion of the fluid property (pressure and velocity). This equation model is semi-empirical, based on the equations of kinetic turbulent energy (k) and the rate of dissipation of kinetic energy (ε), and they can be obtained, respectively by the Eqs. 20 and 21.

$$\rho \frac{\partial k}{\partial t} + \rho \overline{u}_J \frac{\partial k}{\partial x_j} = \frac{\partial}{\partial x_j}\left(\left(\mu + \frac{\mu_t}{\sigma_k}\right)\frac{\partial k}{\partial x_j}\right) + \rho \overline{u_J' u_\iota'}\frac{\partial \overline{u_\iota}}{\partial x_j} - \rho\epsilon \tag{20}$$

$$\rho \frac{\partial \epsilon}{\partial t} + \rho \overline{u}_J \frac{\partial \epsilon}{\partial x_j} = \frac{\partial}{\partial x_j}\left(\left(\mu + \frac{\mu_t}{\sigma_\varepsilon}\right)\frac{\partial \epsilon}{\partial x_j}\right) + C_{\epsilon 1}\frac{\epsilon}{k}\left(\rho \overline{u_J' u_\iota'}\frac{\partial \overline{u_\iota}}{\partial x_j}\right) - C_{\epsilon 2}\rho\frac{\epsilon^2}{k} \tag{21}$$

where $C_{\epsilon 1}$, $C_{\epsilon 2}$, σ_k e σ_ε correspond to the turbulent variables of Prandtl (k) and (ε), with the constant values: $C_{\epsilon 1}$=1,44, $C_{\epsilon 2}$=1,92, σ_k=1,0 e σ_ε=1,3 and μ_t, the turbulent viscosity.

From all the definitions of boundary conditions and turbulence model it is created a CFD model based on the control volume shown on Fig. 6. The mesh of the control volume is shown on Fig. 7, preserving the greatest part of the elements on the regions near the walls.
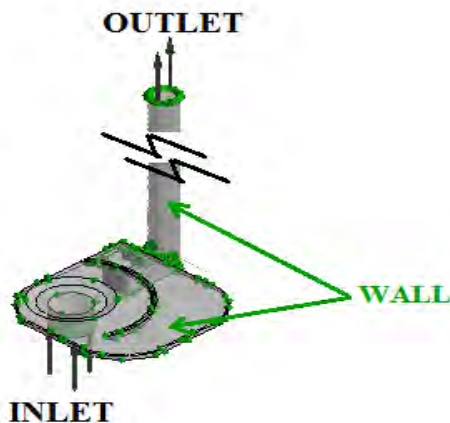
Figure 6. The control volume studied.
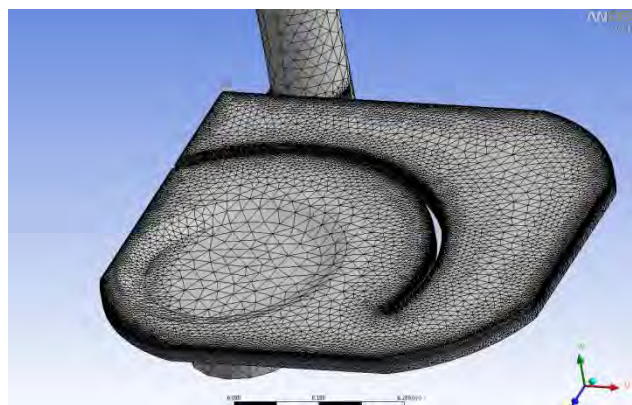
Figure 7. Mesh created for the fluid in the stove.

3.4 Numerical simulation

The CFD calculation (solution to continuity, momentum and turbulent equations) was used in order to export the temperatures on the plate from fluid convection. The results for temperature were exported to the elastothermal model as boundary conditions. The stress suffered by the plate is derived from the temperature gradient distributed over the same in 3 directions. For a complete model it is necessary to inform the material properties of the plate, these are shown on Table 5.

Table 5. Experimental results for gases analysis.

Material	Aluminum	Iron Cast (%C 3 - %Si 2)	Ceramic
Dimension (mm)	Ø 95 x 3000	565 x 565 x 20	575 x 575 x 365
Density (kg/m^3)	2700	7800	4800
Conductivity (W.m-1.K-1)	237	100	Adiabatic (hypotheses)
Fusion Temperature (K)	930	1573	2273
Poisson's Ratio	0.33	0.25	0.2
Young's modulus (GPa)	69	120	250
Lame module (10^9)	50.4	48	69.4
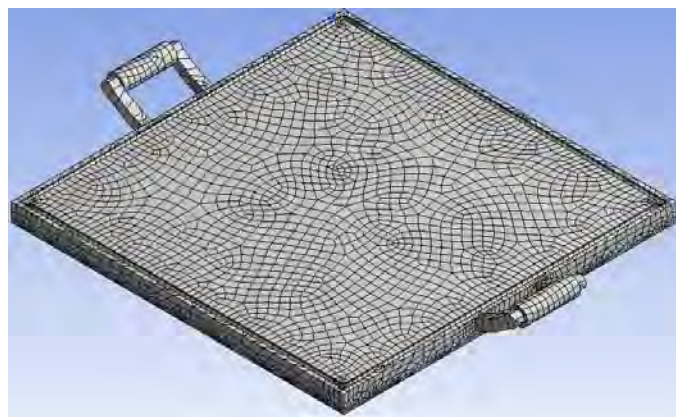
Figure 8. Mesh of the stove plate for elastothermal analysis.

The converged mesh of the stove plate for the elastothermal analysis is shown on Fig. 8, with 124438 nodes. The complete temperature field on the surface of the plate, obtained by combining all heat transfer phenomena is shown on Fig. 9. The experimental data for 90 minutes of consumption of biomass was interpolated for all the surface and is shown on Fig. 10 for the same color map values of Fig. 9.

The numerical results showed quite an acceptable agreement with the experimental data. Even with the need of more measuring points to determine a complete temperature field, on the points measured, the temperature is similar.
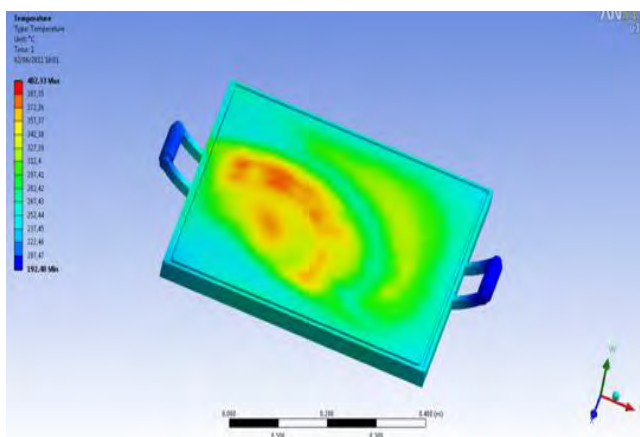
Figure 9. Temperature field on the surface of the plate.
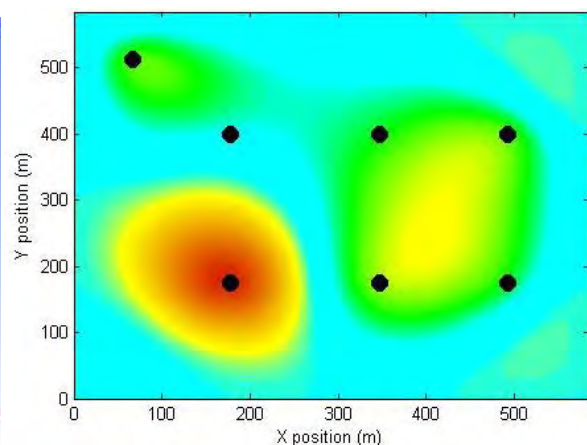
Figure 10. Experimental results interpolated.

Also can be seen by the results, that the heat transfer mode that offers the most potential for efficiency gains is convection. This is achievable by either increasing surface area of the pot exposed to hot combustion gases or by modifying the characteristic flow parameters of mass flow rate and temperature. Temperature has a significantly larger impact on heat transfer than mass flow rate, both through its direct effect on temperature difference and also through the indirect effect it has on convection coefficient.

4. RESULTS AND DISCUSSION

4.1 Stress and deformation analysis

This approach is used when the stress and strain distribution in a model depends on the temperature field of the model whereas temperature distribution can be established without the availability of stress/mechanical strain distribution in the model. The thermal-mechanical problem is solved by first calculating the heat transfer analysis from which we get temperature distribution. For the stress analysis simulation, the nodal temperature data are read from the output file of heat transfer analysis simulation, and are applied on the model as a nodal temperature field in ANSYS WORKBENCH by using predefined fields.

The parameters which influence the performance of a cook stove can be listed mainly in two groups, namely, geometric and thermal parameters. Typically, the geometric parameters consist of size of inlet/outlet ports and the dimensions of combustion chamber while the operating parameters include power, type of fuel, fuel bed porosity etc. In the present analysis, the effects of heat conduction on a stove have been computed, from radiation, convection e conduction phenomena. Further, stove performance on operating is also evaluated based on heat transfer rate to the plate to prevision crack failure by elastothermal analysis.

From the temperature field, it is possible to generate the stress values acting on the stove. It was determined the stresses and the deformation suffered by the stove, which is shown on Fig. 11 and 12, respectively. The maximum stress calculated is 0.188 MPa, giving a safety factor of 1.28, very low since it was considered several simplifying assumptions. In this static analysis were considerate just temperature field by CFD, without displacement boundary condition.
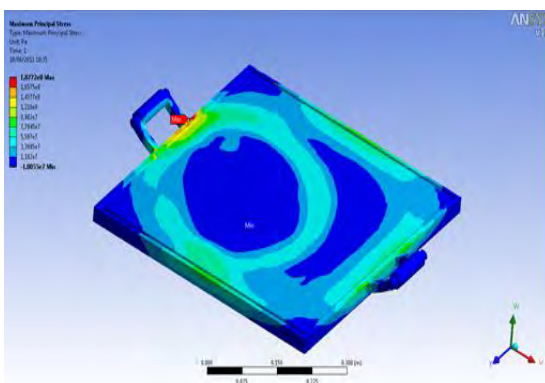
Figure 11. Stress contours on stove plate.
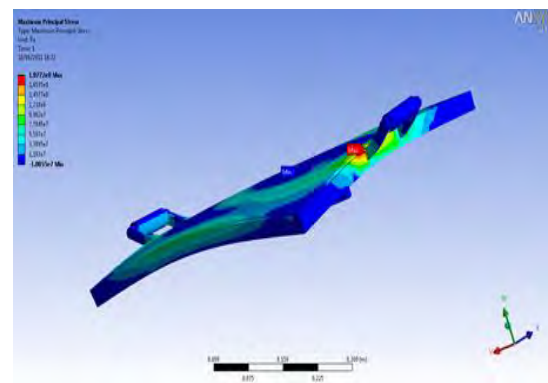
Figure 12. Displacement form on the plate.

4.2 Rupture study on the plate

The studies performed on the laboratory dependencies resulted on the rupture of the plate in use, similarly to the manufacturer reports (see Fig. 13). The structural crack caused by dilation from high temperatures in which the plate is submitted, created two hypotheses to evaluate this situation. One hypothesis is related to material failure only, from badly performed manufacturing process, with pollutants penetration, interstices formations, creating an anisotropic material. And other related to project failure, in which the channeler, that directs the gases flow, impairs a free and uniform dilatation. It was withdrawn a sample of the plate, and there were made several analysis to determine the reason of failure, in order a microstructure analysis, and a chemical scanning to identify the concentration of critical chemical elements, they will be presented below.
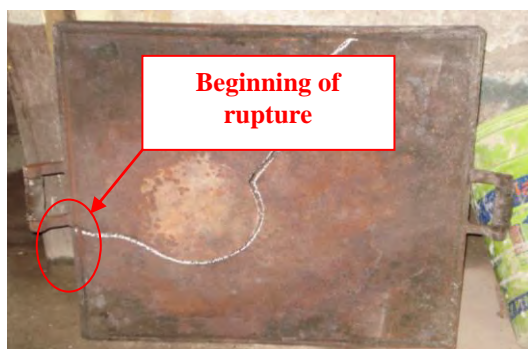
Figure 13. Rupture generated through the plate.

Figure 14. Details of the rupture of part.

With a preliminary visual analysis, could be seen how the rupture occurred on the part and it revealed the shape of the vermicular veins of the microstructure (Fig. 14). The microscopic images shown on Fig. 15, 16, 17 and 18 shows a similarity with gray cast iron due to the graphite vermicular shape. The whitish regions indicate the presence of other chemical elements in higher concentrations that is required by the norm.

Figure 15. Microstructure of rupture center on plate with 50x increase.

Figure 16. Microstructure of rupture extremity on plate with 50x increase.

Figure 17. Microstructure of rupture center on plate with 100x increase.

Figure 18. Microstructure of rupture extremity on plate with 100x increase.

By the chemical analysis, is observed on Table 6, that the concentration of silicon is highly elevated, 235% higher than the required by norm (2%), which means a exacerbated graphitization. The concentration of sulfur, expected to be high, remained within the required. By the metallographic analysis, is observed a type of vermicular graphite quantitatively high, confirming the graphitizing action of silicon. Therefore, the cast iron with high concentration of graphite may present a weaker structure to actions from thermal variations, required to this type of component of the stove.

Table 6. Highlighted elements in chemical scanning.

Chemical elements							
Concentration (%)	Carbon	Silicon	Manganese	Sulfur	Phosphorus	Chrome	Nickel
Specified elements	2.5-4	1-3	0.3-1	0.05-0.25	0.1-1	-	-
Mean from the elements on plate	3.8	4.70	0.22	0.01	0.06	1.23	0.0055

5. CONCLUSION

In the present study, influence geometric and operating parameters related to wood stove have been analyzed in the context of stove structural performance, thermoelasticity, by conducting a numerical simulation of buoyancy induced flow in the chosen stove geometry and after thermal load applied on plate. Approaching heat transfer efficiency of biomass cook stoves from a perspective rooted in the fundamental physics of its operation has proven to be useful in understanding why certain design strategies are more successful than others.

The results of the measurements show that nitrogen makes up the majority of the gas, about 70 % in mass, therefore it will be assumed to be the single component of the fluid on CFD simulation. To calibrate the numerical results were used the experimental data, which showed acceptable agreement.

From a converged structural mesh with 124438 nodes the temperature field was applied, it is possible to generate the stress values acting on the plate of stove. Based on maximum stress criterion, also known as the normal stress, he stresses and the deformation were determined, which showed the maximum stress calculated is 0.188 MPa, giving a safety factor of 1.28, very low since it was considered several simplifying assumptions.

The studies performed on the laboratory dependencies resulted on the rupture of the plate in use. The microstructure and chemical analysis indicate the presence of other chemical elements in higher concentrations that is required by the norm. The structural crack caused by dilation from high temperatures in which the plate is submitted, created two hypotheses to evaluate this situation. Both situations were proved as possible in this paper. Thus, the bad manufacturing process and/or the channeler design (uniform dilatation optimization) can be responsible.

Finally, the structural simulations based in FEM allied to CFD simulations providing subsidies to the plate design to resist better the generated stresses, avoiding cracks, warping and even facilitate the specification of materials most suitable for working conditions. The culmination of all the projects will, it is hoped, result in a set of model equations and a design procedure that would help stove designers take real effects into account in the design of improved woodstoves.

6. REFERENCES

Kohli, S., 1992. *Buoyancy-induced Flow and Heat Transfer in Biomass Stoves,* Ph.D. thesis, Indian Institute of Science, Bangalore, India.

Kohli, S., Srinivasan, J., and Mukunda, H.S., 1993. ''Heat transfer to a horizontal disc using a buoyancy-induced jet''. In *International Journal of Heat and Mass Transfer,* 36(16), pp. 4046-4066.

Kohli, S., Ravi, M.R., and Subbarao, R., 2002. ''Mass flow measurement in buoyancy-induced flow through a vertical tube''. In *Proceedings of the Fifth ISHMTASME Heat and Mass Transfer Conference*. Saha, S.K., Venkateshan, S.P., Prasad, B.V.S.S.S., and Sadhal, S.S., (eds.), pp. 796-801.

Zube, D. J., 2010. *Heat transfer efficiency of biomass cookstoves*. Master of Science thesis. Department of Mechanical Engineering, Colorado State University. Fort Collins, Colorado.

Gupta, R. And Mittal, N. D, 2010. Fluid flow and heat transfer in a single-pan wood stove. In *International Journal of Engineering Science and Technology*, Vol. 2(9), 4312-4324 p.p.

Aziz, A. and Tao, J., 2012. Simulation of Thermal Stresses in a Disc Brake. Master's degree. School of Engineering in Jönköping, Product Development and Materials Engineering. The work is a part of the.

Ravi, M.R.; Kohli, S. and Ray, A., 2002. Use of CFD simulation as a design tool for biomass stoves. *Energy for Sustainable Development* l Volume VI No.

Bhandari, S., Gopi, S., Date, A, 1988. Investigation of CTARA wood-burning stove. Part I. Experimental. *Sãdhanã*, Vol. 13, Part 4, December, pp. 271-293. Printed in India.

Mackin, T.J. and S.C. Noe et al., 2002. Thermal cracking in disc brakes. *Engineering Failure* Anal., 9: 63-76.

7. RESPONSIBILITY NOTICE